INSTITUTE OF PHYSICS PUBLISHING JOURNAL OF PHYSICS: CONDENSED MATTER

J. Phys.: Condens. Matter **16** (2004) S5191–S5202 PII: S0953-8984(04)85838-7

Experimental determination of order in non-equilibrium solids using colloidal gels

Yongxiang Gao and Maria Kilfoil

Department of Physics, McGill University, Montreal, H3A 2T8, Canada

E-mail: kilfoil@physics.mcgill.ca

Received 3 September 2004, in final form 10 September 2004
Published 22 October 2004
Online at stacks.iop.org/JPhysCM/16/S5191
doi:10.1088/0953-8984/16/44/016

Abstract

The idea of quantifying order in disordered systems has been introduced recently by Torquato and co-workers (2000 *Phys. Rev.* E **62** 993–1001). We are interested in the application of this idea to measure structure in non-equilibrium systems. Here we focus on gels, using as a model system colloidal gels formed from hard spheres with polymer added to the systems to induce a controlled, weak attraction. To describe the structure of the gels we use real space imaging via confocal microscopy to obtain the full three-dimensional structure. We measure experimentally both translational order and bond angle correlations, defining a new (refined) translational order parameter that is sensitive to long range order in these non-random packings. This metric is also sensitive to anisotropy, which should be important in the many physical situations where an external force is present. The bond angle distribution shows coordinated organization. To give a clearer physical picture for gels, we compare the experimental data to computer generated hard sphere systems.

(Some figures in this article are in colour only in the electronic version)

1. Introduction

Gels are networks of weakly attractive constituents that are formed from building blocks that are soluble or dispersed in suspension. The networks assume configurations that guarantee mechanical stability, on experimental or functional timescales, in many cases. Other gels are transient networks that reorganize actively in response to external stimuli, as in actin cytoskeletal networks [2], or in a passive fashion before collapsing under their own weight [3]. The gel network must be subject to internal regulation mechanisms that allow its organization into a network that fluctuates while retaining its mechanical integrity. We wish to understand the control mechanisms that determine the structure, the mechanical rigidity, and, ultimately, the long time dynamics. A colloidal gel is an excellent model system for approaching this goal.

Colloids are well-characterized model systems. They can be made repulsive, attractive, or hard sphere-like. They can also be made to form non-equilibrium structures such as gels and glasses by tuning their interactions. They are an excellent realization of atomic systems, as their interactions may be tailored to mimic atomic pair interactions; however, they are large enough ($\sim$1 μm) and slow enough to change (diffusion times of $\sim$ms to s) that we can directly observe them in real time using microscopy and make quantitative measurements of their structure and dynamics [4]. Colloidal gels, like any gels, are sample spanning networks composed of constituents that are made to interact strongly.

We visualize the structure by confocal microscopy and use feature finding algorithms allowing precise location of the centre of mass for all the particles via stacks of images taken at controlled time intervals. These methods provide the full 3D structure. On the timescale of a single stack of images, the structures are arrested; hence this method is well suited for study of the gel structure. We begin the structural analysis by calculating for the gels a translational order parameter previously suggested by Torquato *et al* [5] for identifying non-equilibrium hard sphere packings [1, 5]:

$$T_{\mathrm{s}}^{*} = \frac{1}{r_{\mathrm{c}} - \sigma} \int_{\sigma}^{r_{\mathrm{c}}} |g(r) - 1| \, \mathrm{d}r, \tag{1}$$

where σ is the diameter of the sphere and r_{c} is a cut-off distance that ensures integration over an equal number of coordinate shells across configurations with different particle densities. The central element for the translational order parameter, the radial distribution function (RDF) $g(r)$, measures at what distance a pair of particles prefer to be separated relative to the situation for an ideal gas. $g(r) - 1$ provides a measure of the deviation of the structure from that of an ideal gas. Any deviation from ideal gas will give a corresponding contribution to the integral in (1). The important, novel Torquato translational order parameter is not appropriate for systems with some short range to mid-range order. Such systems call for careful treatment with any order metric, to ensure proper weighting of the structure on different length scales. Nevertheless, T_{s}^{*} can be adapted to handle this weighting correctly, as we have done here, and in this new form it can also be recast such that it is sensitive to anisotropy.

We also measure the nearest neighbour bond angle distribution in the gels. The bond angle distribution measures the local relative orientation of nearest neighbours. We calculate the distributions of those angles from the experimental data. The treatment is novel and the effects discussed will be of particular interest in systems with strong interparticle attractions.

2. Experimental details

We use in our experiment colloidal PMMA spheres whose diameters are 1.26 μm, sterically stabilized with a PHSA 12-carbon layer grafted onto the surface of the particles. We add a controllable interparticle attraction to the system, via depletion [6], through the addition of polymer. The range of the interparticle potential depends on the size of the polymer in the suspending fluid, and the depth of the potential well at contact on the polymer concentration and on the size asymmetry between the polymer and colloid, offering a degree of control over the range and depth of the potential. In the present work, we use a solution of polystyrene chains of a particular, well-defined molecular weight with a mean end-to-end distance of 91 nm in solution to control the potential well. Care is taken to use proper scaling of the size of the polymer at sufficiently high concentrations where the polymer chains interact with each other [7]. The resulting pair potential is shown in figure 1 (*left*). We use a mixture of decalin and tetralin to match the refractive index of the colloidal PMMA particles, enabling observation by laser scanning confocal microscopy deep into the sample to obtain high resolution images.

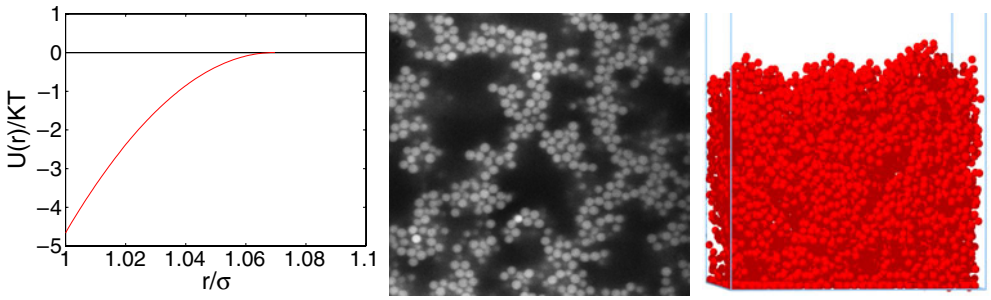

Figure 1. *Left:* the Asakura–Oosawa depletion potential for gel1, plotted as a function of interparticle separation. Distance is normalized to the colloidal particle diameter σ. *Middle:* a typical 2D image from a stack of images through the gel, at 18 μm depth into the sample from the cover slip, illustrating the connectivity of the colloidal gel network. *Right:* the reconstruction obtained from a stack of two-dimensional images acquired at successive focal planes spaced 0.5 μm apart along the vertical direction.

To prepare gels, we start with a low volume fraction of colloids added to the desired polymer solution. After aggregation and sedimentation, the colloids form a weak solid-like network which has a low volume fraction. We use a confocal (inverted) microscope to scan the sample from the bottom to the top in steps of 0.5 μm. The field of view here is 41 μm $\times$ 44 μm. Typically we image 65–100 μm depth. Figure 1 (*middle*) shows a cross-section through the gel showing the connectivity through the colloidal gel network. The algorithms that we use to extract the features from the images are written in Matlab and are based on the algorithms established by Grier and co-workers [8]. The coordinates of each of the 8900 particles are obtained to a precision of $\sim$20 nm. Thus we gain the full 3D structural information. Figure 1 (right) shows a reconstructed volume of the colloidal gel.

We image at controlled, timed intervals of $\Delta t = 5$ min for 2 h. From volume reconstructions that we perform with the full particle-by-particle structural data, we observe that the structure appears static over this timescale. The solid that we observe, while not in *thermodynamic* equilibrium, is in *mechanical* equilibrium. The density profiles up through the sample, calculated from the full single-particle structural data, also exhibit evidence that there are no large scale structural rearrangements, although there is evidence of small, local relaxations in the structure on the timescale on which we observe. This results in fluctuations in otherwise constant density profiles over time. Remarkably, the structure forms at a volume fraction much lower than that required for random packing of non-interacting spheres.

For comparison to experimental data on gel structures formed from attractive, non-penetrating spheres, we generate equilibrium hard sphere configurations as a reference state, using an algorithm based on the Clarke and Wiley (CW) algorithm [9]. This algorithm starts with a randomly distributed configuration of non-overlapping hard spheres at an initially much lower volume fraction and cycles through increasing the radius of all the particles uniformly while moving them to ensure no overlap, until the desired volume fraction is reached. The system is equilibrated by standard molecular dynamics. In each configuration generated, the number of particles is 1000, and all the results based on simulated HS are averaged over roughly 1000 configurations to give good statistics.

3. Translational order parameter

The central element of the translational order parameter that we use is the radial distribution function (RDF), $g(r)$. We measure the full 3D $g(r)$ microscopically. For extracting the RDF

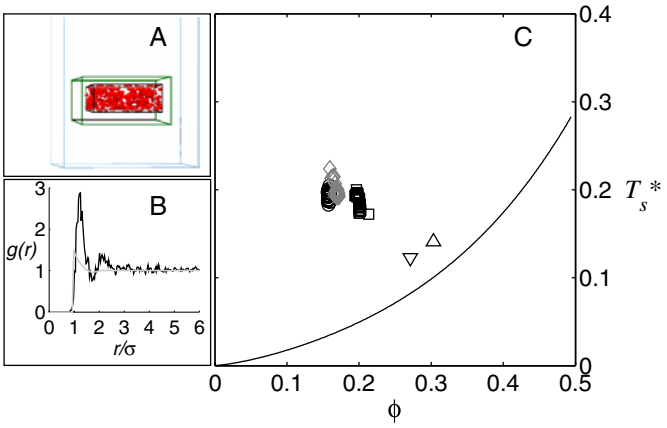

Figure 2. (A) The geometry used for calculating the RDF in the volume of particle coordinates of a colloidal gel. (B) Radial distribution functions for gel (——) and reference state hard sphere fluid (– – –) at the same particle volume fraction, $\phi = 0.156$. The gel data are obtained microscopically from colloid–polymer systems using confocal microscopy, while the hard sphere fluid is generated via computer using the C–W algorithm. (C) T_s^* as obtained from (1). Symbols represent the experimental data. ○: gel1 at $U_0 = 4.2kT$ at contact; ◇: gel2 upper box, also at $U_0 = 4.2kT$ at contact; □: gel2 lower box; and △: gel3 lower box, ▽: gel3 upper box, formed at $U_0 \sim 4kT$ and a shorter range of attraction. The solid curve is T_s^* for non-interacting hard spheres, computed from Percus–Yevick integral equation theory.

from the microscopic data, we select two concentric subvolumes in our volume of particle coordinates that allow us to extend the calculation of the local particle distributions to 8 μm or six particle diameters in each dimension. The geometry of this scheme is depicted in figure 2(A) for the gel data reconstructed in figure 1 (*right*). We calculate the radial distribution function for those particles in the inner box. The choice of box sizes is a compromise to obtain good statistics while restricting the analysis to a well-defined region away from the edges of our field of view and, particularly, well removed from the sample cell wall. A typical gel RDF, from gel1, is shown in figure 2(B). A typical liquid $g(r)$ from a set of configurations of hard spheres at the corresponding packing density is also shown in figure 2(B). Clearly, there is much more structure on the length scale of a few particle diameters in gels than in hard spheres at the same density.

Previous authors have used a translational order parameter based on the integration of $g(r)$ over a scalar radial coordinate, written as (1). We have computed T_s^* from the microscopic data for three different gels: two at the same range and strength of interparticle attraction but differing in starting volume fraction of colloidal particles; and a third with a shorter range of attraction. We label these as 'gel1', 'gel2' and 'gel3'. With 20 configurations obtained experimentally at controlled time intervals for gel1, and 20 configurations for gel2 each affording two completely uncorrelated boxes within the volume, we realize 20 and 40 data sets, respectively, for extracting T_s^* for these structures. For gel3 only one configuration was obtained experimentally. The pair potential at contact, U_0 ($=U(\sigma)$), is $4.2kT$ for gel1 and gel2, and $\sim 4.0kT$ for gel3, with the range of the attraction $1/14$ of the colloidal particle diameter, σ, for gel1 and gel2 and $(1/17)\sigma$ for gel3.

Applying the Torquato translational order metric to our experimental gel systems, we are not able to distinguish from experimental noise any change in T_s^* with increasing r_c when r_c is at least five particle diameters; hence we find that for practical purposes this integral converges for the gels. Figure 2(C) shows that gels have a higher degree of order as measured

Table 1. A summary of results from translational order parameter calculations for the colloidal gels, compiled for both the scalar and volume integral forms of T^*. σ, the standard deviation in the value of T^* averaged over configurations, is a measure of the error.

	ϕ	T_s^*(gel)	σ	T_s^*(P–Y)	$\frac{T_s^*(\text{gel})}{T_s^*(\text{P–Y})}$	T_v^*(gel)	σ	T_v^*(P–Y)	$\frac{T_v^*(\text{gel})}{T_v^*(\text{P–Y})}$
gel1	0.159	0.194	0.006	0.034	5.65	0.071	0.004	0.005	13.7
gel2[a]	0.168	0.200	0.009	0.038	5.32	0.083	0.004	0.006	14.0
gel2[b]	0.200	0.186	0.009	0.049	3.78	0.080	0.004	0.009	9.00
gel3[a]	0.271	0.123	0.006	0.082	1.50	0.055	0.003	0.020	2.84
gel3[b]	0.303	0.141	0.006	0.100	1.40	0.059	0.003	0.027	2.19

[a] Top.
[b] Bottom.

by this order metric: in the plot of T_s^* as a function of ϕ, they are well separated from hard sphere fluid results calculated according to Percus–Yevick integral equation theory [10]. The Torquato *et al* order metric is sensitive to and able to distinguish the difference in short range order between gels and hard spheres, and hence is a useful order parameter for application in this system with attractive interactions.

We redefine this order metric in terms of a volume integral over $g(r)$:

$$T_v^* = \frac{1}{\frac{4}{3}\pi(r_c^3 - \sigma^3)} \int_\sigma^{r_c} |g(r) - 1| 4\pi r^2 \, \mathrm{d}r. \tag{2}$$

In our case, we choose $r_c = 3.5/\rho$, where ρ is the number density. This new translational order parameter is physically appealing, as thermodynamic properties of an isotropic fluid, notably internal energy and pressure, are directly related to a volume integral over $g(r)$ [11]. It more strongly distinguishes the degree of order in local packing density in attractive, gelled particles from that in non-interacting hard spheres. Comparing to the scalar integral, we find that T_v^* measured for the gels, shown in figure 2, differs even more markedly from its value evaluated for the corresponding hard sphere system. The ratio to hard spheres for the same volume fraction is consistently 2–3 times larger using the volume integral-based order metric. The results for T_s^* and T_v^* are summarized in table 1.

Moreover, because T_s^* involves the scalar integral of $g(r)$, its evaluation weights shells equally with increasing scalar radial coordinate. It does not count each particle equivalently in its contribution to the order parameter. Thus the scalar version tends to suppress the order contribution from length scales beyond the length scale of a single particle, and biases the result to short range order by suppressing the contribution from long range order according to $1/r^2$. While the integral converges above five particle diameters, we find that it does not converge over fewer shells. Hence, for smaller cut-off distances, the value of the metric is very sensitive to the choice of cut-off distance and it becomes important to weight the contribution to the integral correctly.

For gels at the same attractive strength and range (gel1 and gel2), the small difference in initial colloid volume fraction has no real effect on the structural parameters. By contrast, both figures 2(C) and 3 show that with decrease of the range of attraction, the value of this translational order metric for gels tends to approach that of the non-interacting hard spheres. This agrees with what one expects, as with a shorter range of attraction, particles exhibit structure more similar to that of hard spheres. However, it is not clear how such an attractive system should approach non-interacting hard spheres; it should be highly dependent on the path taken in control parameter space and this should be reflected in the order metric T^*. We will return to this point below during discussion of the short range orientational order in the gels.

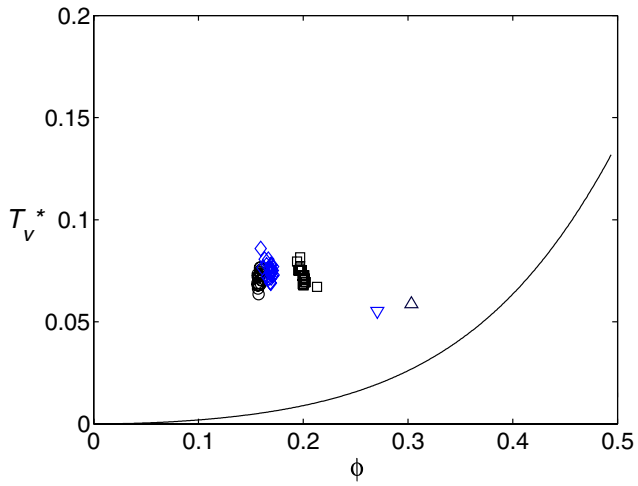

Figure 3. The order metric T_v^* for gels and for non-interacting hard spheres. Symbols represent the experimental data according to the scheme used in figure 2. The solid curve is T_s^* for non-interacting hard spheres, calculated using Percus–Yevick theory.

This new order parameter can be extended to a more general one based on an angular distribution function $g(r, \theta, \phi)$ via

$$g(r) = \frac{1}{4\pi r^2} \int_0^{2\pi} \int_0^{\pi} g(r, \theta, \phi) r^2 \sin\theta \, \mathrm{d}\theta \, \mathrm{d}\phi \qquad \text{and} \tag{3}$$

$$T_v^* = \int_\sigma^{r_c} 4\pi r^2 \left\{ \frac{1}{4\pi} \int_0^{2\pi} \int_0^{\pi} |g(r, \theta, \phi) - 1| \sin\theta \, \mathrm{d}\theta \, \mathrm{d}\phi \right\} \mathrm{d}r, \tag{4}$$

so the order metric will be sensitive to anisotropy. This should be important for detecting any structural bias arising under the influence of a uniaxial pressure [12]. The scalar integral-based translational order parameter cannot be extended to a more general expression that retains the full angle dependence of $g(r)$. These virtues of T_v^* make it a good order parameter.

4. Bond angle distribution

The method of Steinhardt *et al* using a decomposition of the local arrangement of particles into spherical harmonics is an effective way to pick out local and global orientational order in the packing of atoms or of non-interacting hard sphere particles [13]. Indeed, this method provides a signature for identifying the particular lattice structure present in crystalline solids, *in homogeneous systems*. One compelling idea is to extend this method to the gel colloidal structures formed from interacting (attractive) particles. However, any local surface particles existing in the calculation tend to enhance the degree of local order per particle. In attempts to distinguish the gel structure from random packings using this method, we have not seen the sensitivity of the different orders of spherical harmonics to the local order that is clearly evident in the colloidal gel networks.

To describe the orientation of bonds in gel systems, we introduce the $\sin\theta$-normalized bond angle distribution. First we define 'bonds' as the lines connecting nearest neighbour particles. The nearest neighbours of any given particle are those particles lying within the first coordinate shell, determined by radial distances σ to 1.4σ. A given particle i together with two nearest neighbours j and k forms a bond angle with the central particle as the vertex, represented in the

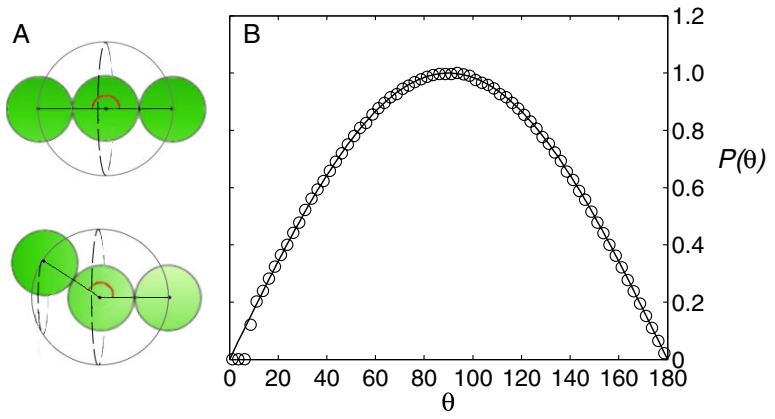

Figure 4. (A) The angle formed by three non-interacting particles, determined purely by entropy. The probability $P(\theta) \propto \sin(\theta)$. (B) The distribution of nearest neighbour bond angles for simulated hard spheres in the low density limit is precisely that of an ideal gas, except at very small angles which are disallowed due to the sphere impenetrability.

inset of figure 5. The angle for the triplet is calculated as $\theta = \cos^{-1}[(\vec{R}_{ij} \cdot \vec{R}_{ik})/|\vec{R}_{ij}||\vec{R}_{ik}|]$. The bond angle distribution is related to the triplet correlation function, limited to nearest neighbour interparticle distances. Using the full structural data, we compute the nearest neighbour triplet angles for all the particles in the region of interest. We calculate the distribution of the angles from θ_c to π, bin the data into 72 bins and normalize the distribution in such a way that the probability of a bond angle between θ and $\theta + d\theta$ satisfies

$$\frac{1}{\pi - \theta_c} \int_{\theta_c}^{\pi} \frac{P(\theta)}{\sin(\theta)} d\theta = 1. \tag{5}$$

The lower cut-off of θ_c reflects the non-penetrability of the spherical colloidal particles. Its value would be 60° if the nearest neighbours could be defined to be those particles in perfect contact, with all interparticle distances at σ. With the nearest neighbour distance definition relaxed to 1.4σ, triplet angles smaller than 60° are allowed. In this case, a θ_c of 40° defines the minimum angle impenetrability limit.

The bond angle distribution gives information about the local allocation of particles in orientation. We would expect a dramatic change in this distribution whenever we have a transition involving a change in the packing of the constituent particles—for example, upon undergoing a disorder–order liquid-to-crystal transition of hard spheres [14] or, equivalently, upon undergoing a liquid–solid gel transition induced by weak interparticle attraction. Importantly, the bond angle distribution is independent of any fixed reference frame and instead defines a local plane for each triplet of particles.

To understand the physics of the bond angle distribution (BAD), consider an ideal gas. For an ideal gas, a completely uncorrelated system, the angle formed by three particles is purely determined by entropy. The probability $P(\theta)$ is proportional to $\sin(\theta)$ (for the same reason there is more land at the Earth's equator than at the Earth's poles). We have sketched this in figure 4. Thus for ideal gas, we expect the bond angles to be distributed according to $\sin(\theta)$. Indeed, for simulated hard spheres in the low density limit, shown in figure 4, the distribution of nearest neighbour bond angles is precisely that of an ideal gas, except at the very small angles disallowed due to the mutual impenetrability of the non-interacting particles. Hence we normalize all of our bond angle distributions to the uncorrelated, ideal gas result at the corresponding density, just as one does in the calculation of the radial distribution function.

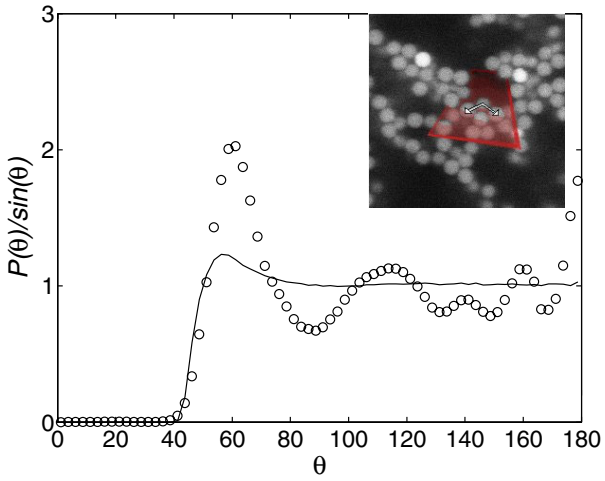

Figure 5. The bond angle distribution $P(\theta)$ discriminates between colloidal gels and non-interacting hard sphere structures. O: $P(\theta)$ for gel1. ——: the bond angle distribution for the corresponding density hard sphere reference system, at $\phi = 0.156$.

The bond angle distribution can be used to distinguish the gel phase. A plot of the bond angle distribution for gel1 appears in figure 5. The bond angle distribution for the corresponding density hard sphere reference system, at $\phi = 0.156$, is also shown for comparison. The degrees of preferred packing are clearly quite different in the two systems. The gel BAD has signatures reflecting enhanced packing at 60°, 120° and, greatly enhanced, at 180°, as well as less prominent but apparently real features at 140° and 160°. These angles can be understood from the nearly equilateral configurations of three particles, in the case of 60°, and a fourth particle between three closely packed particles forcing an angle close to 120°—situations that normally arise in dense packings. Here the particle volume fraction is only 0.16. Nevertheless, these bond angles are easily seen in the gels, for example in the inset of figure 5. The predilection for 180° could arise mainly from the same kinds of adjacent equilateral packings, or from the chains of particles that are evident throughout the gel structure.

With the increase in density of HS fluids, and the accompanying development of short range order *due to packing*, there appears some local crystalline structure, as seen in figure 6. Peaks appear at 60° and 120°, again corresponding to enhanced packing in nearly equilateral configurations. Comparison with figure 5 reveals that gels pack similarly not to hard sphere fluids at the *same* density as the gel, but to much denser hard sphere fluids. However, the key distinction to be made is the following: the attractive hard spheres show some degree of local crystalline order because they are under tension, whereas the non-interacting dense hard sphere fluids show some degree of local crystalline order because they are under compression. The similarities in structure are due to different physics. In addition, gels display short range orientational order not found in the bond angle distribution for a dense fluid, at 140° and at 160°.

The information in the local bond angle distribution among the first shell of neighbours for gel structures is as robust as it is rich. The same signatures are seen: in uncorrelated (separated by distance larger than the length scale over which structure is seen in the RDF) regions in the same gel samples; in different samples prepared under the same initial conditions; and in the same gels over time, subject to density fluctuations. Figure 7(A) shows bond angle distributions $P(\theta)$ for gels prepared at the same range and strength of interparticle attraction

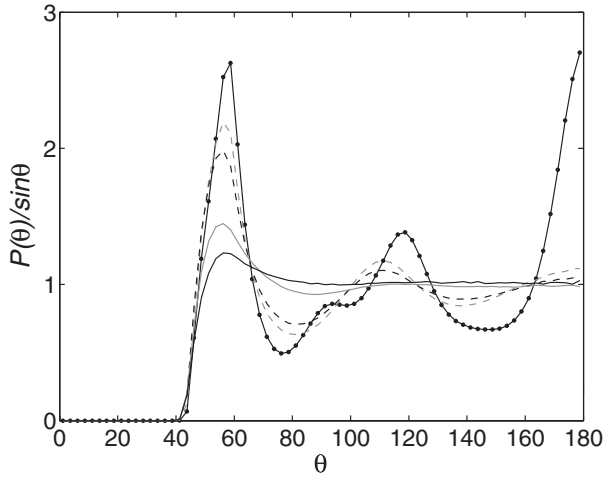

Figure 6. The bond angle distribution $P(\theta)$ for simulated equilibrium hard sphere systems at increasing densities: $\phi = 0.169$ (——), $\phi = 0.294$ (grey ——), $\phi = 0.483$ (– – –), fluids; $\phi = 0.516$ (grey – – –), in the coexistence region with a small degree of crystallization; and $\phi = 0.562$ (–●–), fully crystallized.

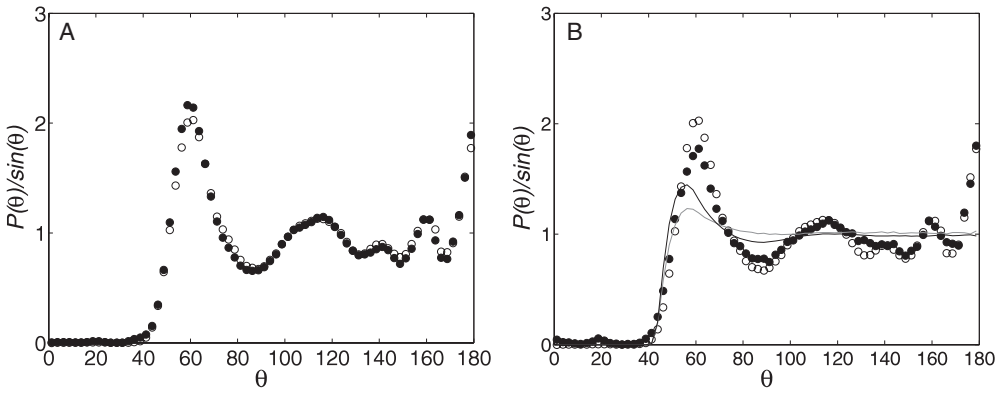

Figure 7. We show that the local orientational order measure $P(\theta)$ is sensitive to internal control parameters of the colloidal gel. (A) Measurements of local orientational order in two gel structures prepared under the same initial conditions of attractive range and strength: bond angle distributions $P(\theta)$ for gel1 (○) and gel2 (●), each prepared at $U_0 = 4.2kT$, $\sigma = 1.3$ μm, range $= (1/14)\sigma$. (B) Bond angle distributions for gel3 (●), range $\sim (1/14)\sigma$, $U_0 = 4.2kT$, $\phi = 0.270$; and gel1 (○), range $\sim (1/17)\sigma$, $U_0 \sim 4.0kT$, $\phi = 0.156$. Also plotted are the bond angle distributions for the hard sphere reference systems at the corresponding densities, obtained from simulated data: $\phi = 0.270$, ——; $\phi = 0.156$, grey ——.

and using the same sizes of colloid and polymer. The bond angle distributions for the two samples are indistinguishable.

Results comparing local structure in two gels with different ranges of attraction are shown in figure 7(B). With the attenuation of the range of attraction, one would expect the features for the bond angle distribution in gels to also become smaller, and features for those gels would be less obvious compared to those for hard sphere systems. We should expect that the weaker the attraction between particles becomes, the more hard sphere-like their behaviour

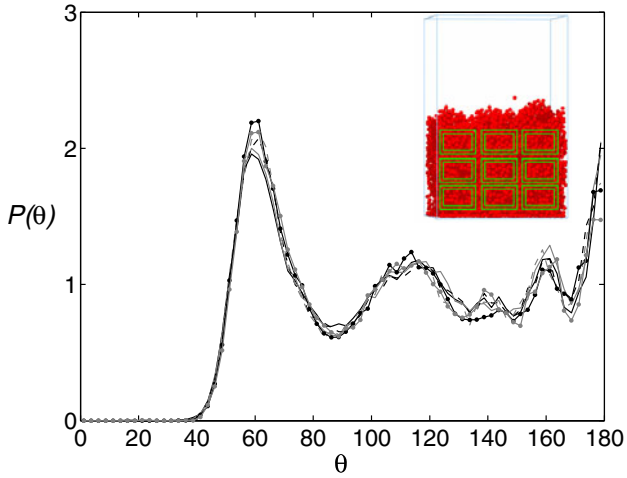

Figure 8. The robustness of apparent signatures of short range order unique to gels. $P(\theta)$ calculated for gel1 for 27 different subvolumes, as represented in the inset, and organized according to the local density in the subvolume: $\phi = 0.23$(——), $\phi = 0.21$ (grey ——), $\phi = 0.19$ (– – –), $\phi = 0.17$ (grey – – –), $\phi = 0.15$ (–●–) and $\phi = 0.13$ (grey –●–).

will become. The situation is more interesting and subtle than this. Two competing effects act simultaneously: that of the higher colloid packing density under weaker attraction, which should tend to cause an increase in intensity of the short range order peaks for the dense hard sphere packing; and that of the weaker gel-like structure and corresponding decrease in intensity of the short range order peaks characteristic of the gel. It is not clear *a priori* which of the two effects will be dominant, or whether in fact they will (coincidentally or by design) exactly cancel for all gels as the strength of the attraction is decreased until purely hard sphere behaviour is reached. At the attractive strength of the one gel studied in this regime, we see in fact a decrease in the intensity of the peaks, shown in figure 7.

To gain some physical insight into the apparent signatures of additional short range order at 140° and 160° in gels that is absent in the short range order in hard sphere systems, we test the robustness of these peaks with respect to density. We study the bond angle distribution within a small box of fixed side length and unique local density at different positions in the sample. The gel structure is subdivided into $3 \times 3 \times 3$ small regions and the calculation carried out for all 20 time-delayed configurations of gel1, resulting (due to fluctuations within individual boxes over time) in 540 boxes in total. We compute an average angle distribution for each density, choosing for comparison only those densities which are found in a significant number of boxes. Peaks which disappear with changing density should be the result of systematic noise, while those which are robust against changing density reflect real packing effects. The results, for local volume fractions ranging from $\phi = 0.13$ to 0.23, are shown in figure 8. We find consistently that the peak at 140° disappears with decreasing density while the unidentified peak at 160° persists. As expected, the crystalline order peaks at 60°, 120° and 180° persist.

This coarse graining approach applied here to correlate preferred local orientation of packing with local density merits further study. For those peaks that persist, this early result reinforces what we have observed in the translational order: it suggests that the attractive force is the internal control parameter that determines the structure. While particle number density determines the total volume of voids and, put simply, the number of particles available

for packing, particle number density has little effect on the packing of the particles which ultimately gives the structure its mechanical rigidity. This is in marked contrast to the case for non-interacting hard spheres, where, as can be seen in figure 6, particle number density completely determines the packing of particles. Intriguingly, it appears that in colloidal systems with depletion attractions of the order of several kT, the depth and range of the attraction are the control parameters that determine the structure.

5. Conclusion

We have quantified the structure of real colloidal gels in two ways: via the translational order parameter and the bond angle distribution. In doing so we have applied the translational order metric proposed by Torquato *et al*, have shown that it is well able to distinguish structure in systems with attractive interactions from that in non-interacting hard sphere systems and have refined this order metric so that it weights all length scales equally in their contribution to the order and is sensitive to anisotropy. It is clear from these results that attractive particles occupy a completely different phase space as compared to non-interacting hard spheres. This work suggests that the depth and range of an attraction added to hard spheres are internal control parameters in determining the structure in colloidal gels and perhaps, by extension, other kinds of gels. As for crystalline solids, it is remarkable that such detail can be found in the local order in the shell of nearest neighbours. The local bond angle distributions reveal that attractive hard spheres build structures such that, under tension, the spheres assume local arrangements very similar to the local arrangements in dense non-interacting hard sphere systems under compression. These arrangements must be intimately related to the mechanical properties and, indeed, may be crucial to the lifetime of the gel.

Acknowledgments

The current work was financially supported by NSERC. We first thank Andrew Schofield and Peter Pusey of University of Edinburgh for providing PMMA latex particles, and Dave Weitz of Harvard University for allowing the use of equipment. We also thank Erik Luijten of the University of Illinois at Urbana-Champaign and Jorge Viñals of McGill University for useful discussions, and Jay Vidyarthi for technical help.

References

[1] Truskett T M, Torquato S and Debenedetti P G 2000 *Phys. Rev.* E **62** 993–1001
[2] Lodish H *et al* 2003 *Molecular Cell Biology* 5th edn (New York: Freeman)
Kreis T and Vale R 1986 *Cytoskeletal and Motor Proteins* 2nd edn (Oxford: Oxford University Press)
[3] Kilfoil M L, Pashkovski E E, Masters J G and Weitz D A 2003 *Phil. Trans. R. Soc.* A **361** 753–66
Starrs L, Poon W C K, Hibberd D J and Robins M M 2002 *J. Phys.: Condens. Matter* **14** 2485–505
Poon W C K, Starrs L, Meeker S P, Moussaid A, Evans R M L, Pusey P N and Robins M M 1999 *Faraday Discuss.* **112** 143–54
[4] Gasser U, Weeks E R, Schofield A, Pusey P N and Weitz D A 2001 *Science* **292** 258–62
[5] Anuraag R, Kansal R, Torquato S and Stillinger F H 2002 *Phys. Rev.* E **66** 0411091
[6] Asakura S and Oosawa F 1958 *J. Polym. Sci.* **33** 183–92
Vrij A 1980 *J. Chem. Phys.* **72** 3735–9
[7] Wiltzius P, Haller H R, Cannell D S and Schaefer D W 1983 *Phys. Rev. Lett.* **51** 1183–6
[8] Crocker J C and Grier D G 1996 *J. Colloid Interface Sci.* **179** 298–310
[9] Clarke A S and Wiley J D 1987 *Phys. Rev.* B **35** 7350–6
[10] Percus J K and Yevick G J 1958 *Phys. Rev.* **110** 1–13
Percus J K 1962 *Phys. Rev. Lett.* **8** 462–3

[11] Hill T L 1986 *An Introduction to Statistical Thermodynamics* (New York: Dover)
Hansen J-P and McDonald I R 1986 *Theory of Simple Liquids* 2nd edn (London: Academic)
[12] Chaikin P M 1999 *Soft and Fragile Matter: Nonequilibrium Dynamics, Metastability and Flow* ed M E Cates and M R Evans (Bristol: Institute of Physics Publishing) (Philadelphia, PA: Scottish Universities Summer School in Physics)
[13] Steinhardt P J, Nelson D R and Ronchetti M 1983 *Phys. Rev.* B **28** 784–805
[14] Haymet A D J, Rice S A and Madden W G 1981 *J. Chem. Phys.* **75** 4696–706